Demonstration of complementary apodized cascaded grating waveguides for tunable optical delay lines

Saeed Khan[1,2] and Sasan Fathpour[1,2,*]

[1]*CREOL, The College of Optics and Photonics, University of Central Florida, Orlando, Florida 32816, USA*

[2]*Department of Electrical Engineering and Computer Science, University of Central Florida, Orlando, Florida 32816, USA*

**Corresponding author: fathpour@creol.ucf.edu*

Received July 15, 2013; revised August 22, 2013; accepted August 23, 2013;
posted August 26, 2013 (Doc. ID 193863); published September 30, 2013

High-speed, tunable integrated silicon photonic delay lines are demonstrated by cascading complementary apodized silicon grating waveguides. The cascaded grating waveguides, with inward and outward super-Gaussian apodization profiles, compensate each other's dispersion and allow high-speed operation. Characterization of the compact delay lines shows that they have low loss, offer true time delays of 82 ps and a tuning range of 32 ps, and can potentially operate at bit rates as high as 107 Gb/s. © 2013 Optical Society of America

OCIS codes: (250.0250) Optoelectronics; (250.5300) Photonic integrated circuits.
http://dx.doi.org/10.1364/OL.38.003914

Continuously tunable, true-time optical delay lines are important components for a host of photonic systems applications [1–3]. Historically, delay lines based on fiber Bragg gratings (FBGs) have been used. However, a tunable laser is required for tuning the delay in FBGs, i.e., tuning the delay at a fixed operating wavelength is not feasible. Silicon-based integrated true-time delay lines have been alternatively pursued for their compactness and ease of tuning. They were first reported in standard silicon-on-insulator (SOI) waveguides [4]. Some important demonstrated device architectures demonstrated more recently include coupled-resonator optical waveguides (CROWs) [5,6], side-coupled integrated spaced sequence of resonators (SCISSORs) devices [7,8], overcoupled microdisk resonators [9], and photonic crystal (PhC) devices designed specifically for optical delay lines [6,10,11]. Each of these schemes has its pros and cons. For example, CROWs and PhC's have very high bandwidth, but optical loss in CROWs can be as high as 60 dB/ns [6], and in PhC devices it can be 35–100 dB/ns [6,11]. SCISSOR devices offer lower loss and high tunability but suffer from low operational speed [8].

We have recently proposed and theoretically shown that high-speed operation and high tunability can be simultaneously achieved in grating-based delay lines using a dispersion compensation scheme [3]. The scheme is based on cascading two apodized grating waveguides with outward and inward super-Gaussian apodization profiles. This somewhat resembles the scheme utilized in SCISSOR-based delay lines [7,8]. We also note that the slow-light effect in Bragg grating waveguides has previously been utilized in optical modulators [12], where only a small delay, corresponding to a phase shift of π, is required. However, for large delays, of the order of hundreds of picoseconds, the gratings need to be properly apodized to remove group-delay ripples, as discussed below. The proposed scheme has its own merits and drawbacks. It is not as compact as the other approaches mentioned above, but it has less insertion loss compared with CROWs and PhC devices, and with a potential bit rate higher than 100 Gb/s, it is much faster than SCISSOR devices. In this Letter, such complementary apodized cascaded grating waveguides are demonstrated for the first time.

The slow-light effect near the band edge of a grating waveguide can be used to impose a time delay on the optical signal. As shown in Fig. 1(a), if uniform gratings are employed, anomalous and normal dispersion regimes exist at these regions (below and above the stop band). However, group-delay ripples, due to the Fabry–Perot

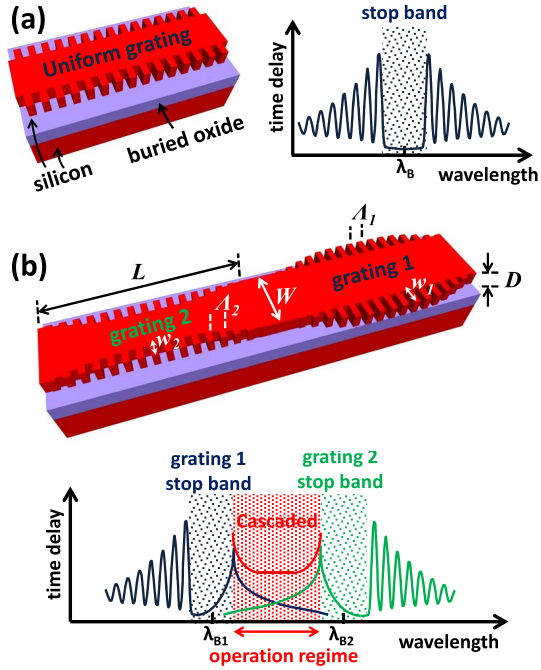

Fig. 1. (a) Schematic of a standard grating waveguide and its delay spectrum. (b) Schematic of cascaded complementary apodized gratings, using an outward-apodized grating (grating 1) and an inward-apodized grating (grating 2). The delay spectra of gratings 1 and 2 are shown in blue and green, respectively. The combined delay spectrum of the cascaded device is shown in red.

cavity formed by the sharp ends of the grating, prevent using the device as an optical delay line in the transmission mode. This problem can be solved by apodizing the grating profile [2], and the performance can be enhanced if two complementary apodized grating waveguides are cascaded [3].

Figure 1(b) schematically depicts such cascaded waveguides and their individual and combined dispersion-compensating delay spectra for transmission-mode operation. The cascaded design consists of two SOI grating waveguides with outward and inward super-Gaussian apodized grating profiles. The effect of outward and inward apodization is to remove the uniform grating ripples at wavelengths above and below the stop band, respectively, such that the inherent normal and anomalous dispersion of the grating waveguides at one edge of the stop band is smoothed. The outward apodization profile, for instance, causes an increase in the grating effective index as the grating width increases. This results in a higher Bragg wavelength for the center of the grating as compared with its wings. At wavelengths above the stop band, where the dispersion is normal, the light no longer experiences the abrupt effective-index transition that exists in uniform gratings [compare spectra in Figs. 1(a) and 1(b)]. Hence, apodization results in smooth transmission and delay spectra in the operation regime shown. Still, the wings of the grating form a Fabry–Perot cavity at wavelengths below the stop band, resulting in huge ripples in that unused wavelength range. Similarly, as shown in Fig. 1(b), the complementary grating waveguide with inward apodization has a delay spectrum that is a mirror image of the outward grating's and has a smooth anomalous dispersion below its stop band.

For either apodization, the time delay can be tuned by changing the refractive index of the core waveguide material (silicon) by changing its temperature, through the thermo-optic effect as demonstrated here or through the electro-optic effect, as we have proposed elsewhere [2]. As the refractive index of silicon increases with temperature, the delay spectra of both grating devices are redshifted. Consequently, the delay of the transmitted light increases with temperature for grating 1 as a result of its normal dispersion. The opposite is true for grating 2.

Figure 1(b) also shows how cascading the complementary apodized gratings can compensate their respective dispersions by taking advantage of their mirror-image delay spectra. By appropriately choosing the center Bragg wavelengths λ_{B1} and λ_{B2}, a relatively flattened dispersion relation can be obtained in the operation regime of the cascaded device (red curve). Consequently, high delay and high bandwidth are simultaneously achievable in the wavelength range between the two stop bands of the cascaded gratings. Furthermore, the cascaded scheme offers high tunability as compared with a single device with the same device parameters and electrical tuning power, as explained below.

Efficient apodization is very important for the cascaded scheme, because it significantly reduces the reflection of the grating interfaces and hence eliminates the undesired Fabry–Perot cavity fringes between the cascaded gratings, which would otherwise drastically reduce the operating speed. Super-Gaussian apodization is chosen here by virtue of its compact tapered regions.

Transmission coefficients of the structures were calculated and optimized by using the standard transfer matrix method [2,3]. The commercial simulation software COMSOL is used to determine the effective refractive index of each corrugated section of the gratings. According to our design, each grating waveguide has a width W of 580 nm and a length L of 2.5 mm. A super-Gaussian apodization function of order 12 with a full width at half-maximum of 1.75 mm is used. Grating 1 has a maximum grating width w_1 of 210 nm and a grating period Λ_1 of 285 nm (Fig. 1). Grating 2 has a maximum grating width w_2 of 65 nm and a grating period Λ_2 of 320 nm (Fig. 1). According to fits to the experimental results presented below, for these design parameters, when grating 1 is 45°C above room temperature (T_R) and grating 2 is at T_R, the upper stop-band edge of grating 1 coincides with the lower stop-band edge of grating 2. Under these conditions ($\Delta T = T_2 - T_1 = -45$°C), the time delay is at its maximum and the bit rate is at its minimum. Varying ΔT to approximately +45°C, i.e., when grating 1 is at T_R and grating 2 is 45°C above that, shifts the delay spectrum to the other extreme of minimum delay and maximum bit rate.

The designed grating waveguides were fabricated in the frame of ePIXfab setup by IMEC vzw CEA using a complementary metal-oxide semiconductor (CMOS) compatible process using 193-nm deep ultraviolet lithography. The employed SOI wafer had a 220 nm thick top silicon layer and a 2 μm thick buried oxide layer. Ti/TiN metallic microheaters 2 μm wide and 110 nm thick were fabricated on top of the grating waveguides for delay tuning. To avoid metallic loss, a 600 nm thick SiO_2 layer was deposited between the microheaters and the silicon ridges. Waveguide grating couplers are used to launch the transverse electric mode of a tunable laser source in and out of the chip via single-mode optical fibers. The fabricated couplers have a grating period of 630 nm, length of 20 μm, width of 10 μm, and corrugation depth of 70 nm.

The grating delay lines are characterized by integrating them in a Mach–Zehnder interferometer (MZI) configuration, in which the actual time delay can be extracted by studying the optical phase properties [13]. In the MZI devices (Fig. 2, blue and red lines), the reference arm contains cascaded grating waveguides similar to our gratings 1 and 2 but with a 5 nm smaller period of 280 nm for the type 1 grating and a 5 nm longer period of 325 nm for type 2 grating. The gratings in the reference arm are used to balance the loss of the arms. Meanwhile, the 5 nm shorter grating period blueshifts its band-edge wavelength by ~20 nm, and the 5 nm larger grating period redshifts its band-edge wavelength by ~10 nm (according to Fig. 2), giving an almost flat reference delay, corresponding to a propagation length of 5 mm at our operating wavelength of 1521.8 nm. The group-delay difference between the signal and reference arms creates interference fringes such that faster fringe oscillation corresponds to longer delay. Mathematically, the signal-arm delay can be accurately extracted from the wavelengths of the maxima and minima of the MZI fringes λ_{max} and λ_{min}, that is, $T_{sig} = \lambda_{min}\lambda_{max}/[2c(\lambda_{max} - \lambda_{min})] + T_{ref}$. Here

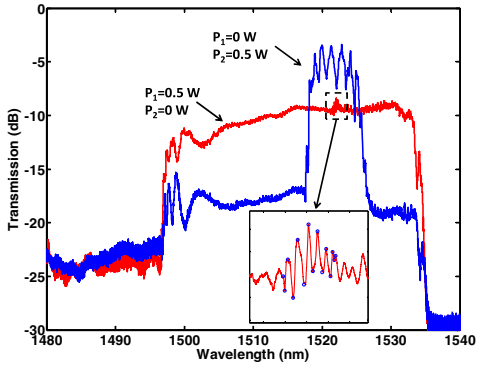

Fig. 2. Transmission spectra of an MZI with gratings. The blue line (with large spikes) is the transmission spectrum when 0 W is applied to the microheater on top of the type 1 grating and 0.5 W is applied to the type 2 grating. The red spectrum is for the opposite electrical power conditions.

c is the speed of light in vacuum and T_{ref} is the delay of the reference arm.

The blue line in Fig. 2 shows the transmission spectrum of a typical MZI device when 0 W of electrical power is applied to the type 1 grating's microheater (P_1) and 0.5 W is applied to type 2's (P_2). Similarly, the red line in Fig. 2 shows the transmission spectrum of a typical MZI for $P_1 = 0.5$ W and $P_2 = 0$ W.

Figure 3 shows the delay spectrum, extracted from the wavelength location of the minima and maxima of the grating waveguides in the MZI configuration, for $P_1 = 0.5$ W and $P_2 = 0$ W (circles). The triangles are for $P_1 = 0$ W and $P_2 = 0.5$ W. The solid lines show the simulation fits to the results, based on the model described elsewhere [2,3]. Here the maximum grating width w is varied to fit the experimental data, while the waveguide width W is set 10 nm less than the value used in the photolithographic mask (580 nm) to account for 10 nm of dry oxidation that was performed for sidewall smoothing. For the type 2 grating, the feature-size values used in simulation were decreased by less than 5 nm on each side from the values used in the photolithographic mask. While this discrepancy may be explained by the contracting effect of the oxidation, the type 1 devices are

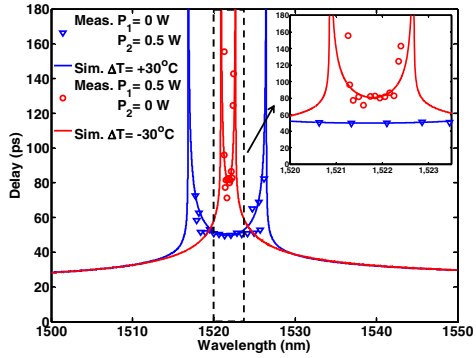

Fig. 3. Delay spectrum extracted from the measured wavelength location of the minima and maxima of the grating waveguides in MZI configuration with grating 1 at 0 W and grating 2 at 0.5 W (triangles) and with 0.5 W for grating 1 and 0 W for grating 2 (circles). Solid lines show the simulation results for the corresponding conditions. $\Delta T = T_2 - T_1$ is the temperature difference between the gratings.

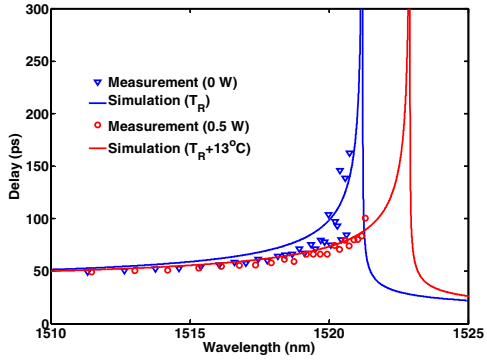

Fig. 4. Delay spectra for a 5-mm-long type 2 grating at different bias powers.

apparently much further off from the design values, since the grating width w_1 had to be decreased by 30 nm to fit the experimental data. This discrepancy seems to be a result of fabrication errors, or it could be due to inaccurate estimation of the refractive index profiles in the COMSOL simulations. The blue line in Fig. 3 was obtained by assuming that $T_1 = T_R$ and $T_2 = T_R + 30°\text{C}$, that is, $\Delta T = +30°\text{C}$. The red line was obtained at $T_1 = T_R + 30°\text{C}$ and $T_2 = T_R (\Delta T = -30°\text{C})$.

To estimate the impact of cascading, the cascaded devices were compared with a single-grating type 2 device, which has a length equal to the sum of the two gratings in the cascaded scheme (5 mm). Figure 4 shows the delay spectra of such a grating at consumed powers of 0 W (blue line, triangles) and 0.5 W (red line, circles). The electrical power was limited to 0.5 W to compare its tunability with a cascaded device at the same maximum tuning power. As discussed below, the cascaded device has a greater tunability range, because 0.5 W is applied to heat a length of 2.5 mm, whereas for the single device 0.5 W will heat a 5 mm grating. This results in an increase in the tunability of the cascaded device.

The limitation imposed by dispersion on the bit rate is estimated from the dispersion fits to the experimental data. Specifically, the bit rate values shown in Fig. 5 are calculated from broadening of transform-limited input pulses of the delay spectra such that 95% of the

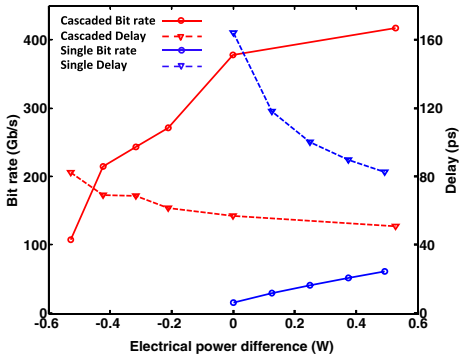

Fig. 5. Bit rate and delay versus applied bias for a cascaded and a single device. For the cascaded device, the x axis is $P_2 - P_1$, where P_1 is the electrical power applied to the type 1 grating and P_2 is the corresponding value for the type 2 grating. For the single device, the x axis corresponds to the power applied to the type 2 grating.

Table 1. Comparison of the Characterized Cascaded and Single Devices

	Cascaded	Single Large Delay	Single Large Bandwidth
Delay	82 ps	164 ps	82 ps
Bandwidth (bit rate)	53.5 GHz (107 Gb/s)	7.5 GHz (15 Gb/s)	31 GHz (62 Gb/s)
Delay × bit rate	8.8	2.5	5.1
Tunability	32 ps	81 ps	14.2 ps
Tunability × bit rate	3.4	1.2	0.88

output pulse energy would stay in its corresponding time slot [2,3]. Non-return-to-zero format is assumed in the bit rate calculations, i.e., the nominal bandwidth of the delay lines is half the reported bit rates. In each calculation, the grating waveguide temperature was adjusted to fit the experimental data for the corresponding bias value.

Thermal cross talk between the two gratings is an issue in this proof-of-concept demonstration. The two gratings were placed 10 μm apart as suggested by a 3D heat diffusion simulation based on COMSOL. The distance between the microheaters is 100 μm. However, by increasing the electrical power beyond 0.5 W in one grating, the spectrum of the other grating shifts too, which is clearly a sign of thermal cross talk. Because of this, we were not able to bring the spectra of the gratings close enough to get a delay above 82 ps. The problem of thermal cross talk can be solved by increasing the gap between the apodized gratings. As we have discussed elsewhere [3], the gap does not affect the combined delay spectrum.

Important figures of merit of the cascaded device are listed in Table 1 and compared with the discussed single device of the same length and under same electrical tuning power. In the cascaded device, a maximum delay of 82 ps and tuning range of 32 ps, with a bit rate as high as 107 Gb/s (corresponding to a bandwidth of 53.5 GHz), were extracted according to the discussed methods. As mentioned, the delay was limited by thermal cross talk. The delay–bit rate product in this device is 8.8 and the tunability–bit rate product is 3.4. The signal wavelength was set at 1521.8 nm (Fig. 3). For the single type 2 device, the signal wavelength is 1520.9 nm, that is, when the tunability–bit rate product is at its highest value of 1.2, corresponding to a delay of 164 ps and a bit rate of 15 Gb/s (7.5 GHz). The tunability range for this case is 81 ps, the delay–bit rate product is 2.5 (~28% of the cascaded device), and the tunability–bit rate product is 1.2 (~2.8 times smaller). The two devices were also compared by assuming a smaller signal wavelength (1519.1 nm) for the single device. At this wavelength, the single-device maximum delay is identical to the discussed cascaded maximum delay of 82 ps. In this case, the bit rate is estimated to be 62 Gb/s (31 GHz) for the single device and the tuning range is limited to 14.2 ps. The resulting delay–bit rate product is 5.1, which is 1.7 times smaller than the cascaded device, and the tunability–bit rate product is only 0.88 (3.9 times smaller than the cascaded device).

For the cascaded device, the insertion loss of the MZI with gratings is 8.4 dB when the delay is at maximum (82 ps). To exclude the losses of the fiber couplers and MZI from the loss calculations for the delay line, a test device without any grating was also fabricated on the same die. The insertion loss of the MZI device without gratings is 5.2 dB. This suggests that the loss induced by the gratings alone at the delay of 82 ps is of the order of 3.2 dB.

In conclusion, optical delay lines based on cascaded complementary apodized silicon grating waveguides have been demonstrated on a CMOS-compatible SOI fabrication process. Their characterization shows that by cascading complementary apodized gratings, an enhancement of around 3 times in tunability–bit rate product is possible compared with a single-grating device. The measured time delay in the cascaded device is 82 ps with a tunability of 32 ps, and the devices can potentially operate at a bit rate of 107 Gb/s.

The work is supported by the U.S. National Science Foundation under award ECCS 1128208.

References

1. G. Lenz, B. J. Eggleton, C. K. Madsen, and R. E. Slusher, IEEE J. Quantum Electron. **37**, 525 (2001).
2. S. Khan, M. A. Baghban, and S. Fathpour, Opt. Express **19**, 11780 (2011).
3. S. Khan and S. Fathpour, Opt. Express **20**, 19859 (2012).
4. S. Yegnanarayanan, P. D. Trinh, F. Coppinger, and B. Jalali, IEEE Photon. Technol. Lett. **9**, 634 (1997).
5. F. Xia, L. Sekaric, and Yu. Vlasov, Nat. Photonics **1**, 65 (2007).
6. A. Melloni, A. Canciamilla, C. Ferrari, F. Morichetti, L. O'Faolain, T. F. Krauss, R. De La Rue, A. Samarelli, and M. Sorel, IEEE Photon. J. **2**, 181 (2010).
7. J. B. Khurgin and P. A. Morton, Opt. Lett. **34**, 2655 (2009).
8. P. A. Morton, J. Cardenas, J. B. Khurgin, and M. Lipson, IEEE Photon. Technol. Lett. **24**, 512 (2012).
9. Q. Li, A. A. Eftekhar, P. Alipour, A. H. Atabaki, S. Yegnanarayanan, and A. Adibi, IEEE Photon. Technol. Lett. **24**, 1276 (2012).
10. Y. Jiang, W. Jiang, X. Chen, L. Gu, B. Howley, and R. T. Chen, Proc. SPIE **5733**, 166 (2005).
11. J. Adachi, N. Ishikura, H. Sasaki, and T. Baba, IEEE J. Sel. Top. Quantum Electron. **16**, 192 (2010).
12. J. B. Khurgin, J. U. Kang, and Y. J. Ding, Opt. Lett. **25**, 70 (2000).
13. Yu. A. Vlasov, M. O'Boyle, H. F. Hamann, and S. J. McNab, Nature **438**, 65 (2005).